Supplementary Information (SI) for Journal of Materials Chemistry A.
This journal is © The Royal Society of Chemistry 2025

Supporting Information

Suppressing Failure Mechanisms in Thick Ni-Rich Cathodes Using Angstrom-Level Alumina Coatings

Surat Prempluem, Thitiphum Sangsanit, Worapol Tejangkura and Montree Sawangphruk*

Centre of Excellence for Energy Storage Technology, Department of Chemical and Biomolecular Engineering, School of Energy Science and Engineering, Vidyasirimedhi Institute of Science and Technology, Rayong 21210, Thailand

E-mail: montree.s@vistec.ac.th

Supporting results

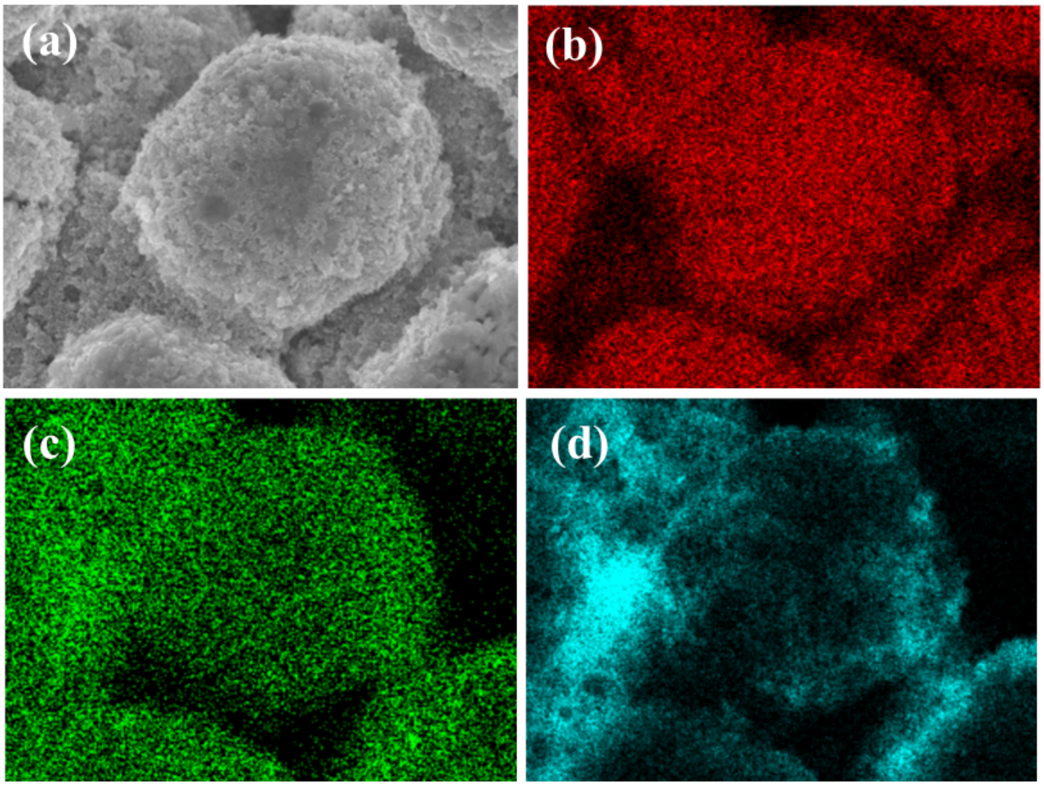

Fig. S1 SEM-EDS mapping of an electrode coated with 10 ALD cycles showing (a) SEM image, (b) Nickel (Ni) signal, (c) Aluminum (Al) signal, and (d) carbon (C) signal.

Table S1. Elemental composition determined by SEM-EDS according to Fig. S1.

Element	Line Type	Apparent Concentration	k Ratio	Wt%	Wt% Sigma
C	K series	1.69	0.01686	32.01	0.09
O	K series	3.78	0.01272	20.80	0.07
F	K series	1.31	0.00257	5.13	0.05
Al	K series	0.10	0.00071	0.77	0.01
Ti	K series	0.06	0.00056	0.36	0.02
Mn	K series	0.71	0.00713	4.42	0.04
Co	K series	0.67	0.00674	4.68	0.05
Ni	K series	4.73	0.04734	31.83	0.10
Total:				100.00	

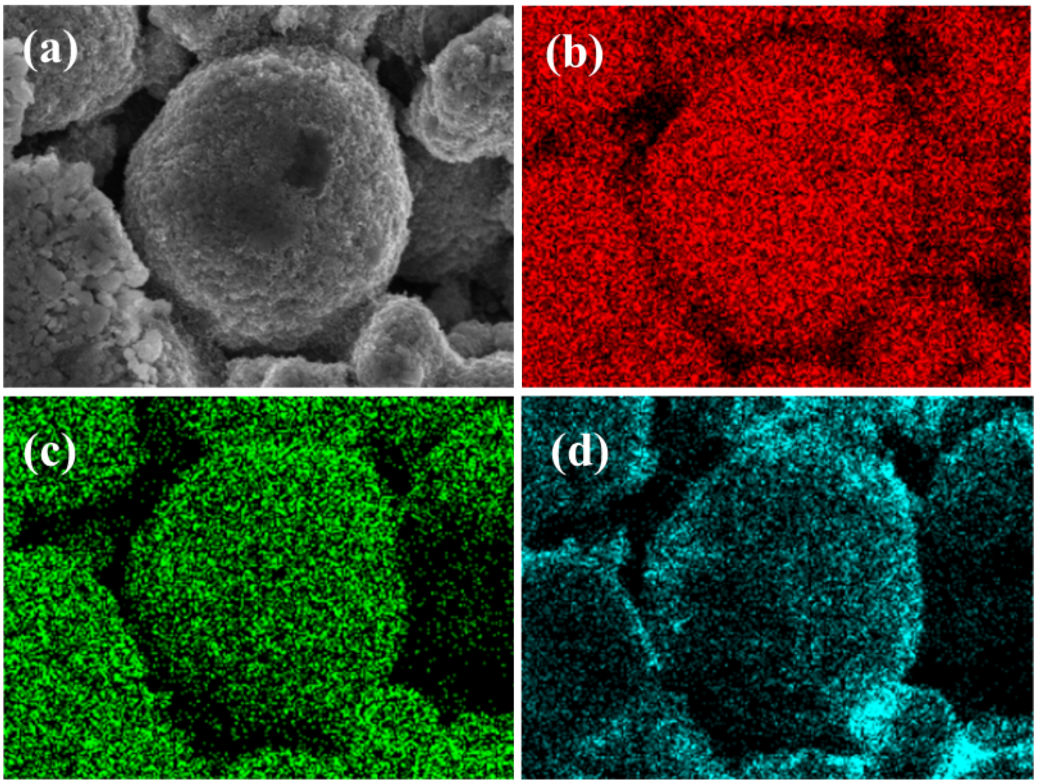

Fig. S2 SEM-EDS mapping of an electrode coated with 25 ALD cycles showing (a) SEM image, (b) Ni signal, (c) Al signal, and (d) C signal.

Table S2. Elemental composition determined by SEM-EDS according to Fig. S2.

Element	Line Type	Apparent Concentration	k Ratio	Wt%	Wt% Sigma
C	K series	0.22	0.00221	16.42	0.14
O	K series	1.86	0.00624	25.98	0.11
Al	K series	0.06	0.00043	1.62	0.03
Si	K series	0.00	0.00001	0.02	0.02
Ti	K series	0.02	0.00018	0.36	0.03
Mn	K series	0.32	0.00315	6.04	0.07
Co	K series	0.29	0.00288	6.21	0.10
Ni	K series	2.08	0.02079	43.37	0.17
Total:				100.00	

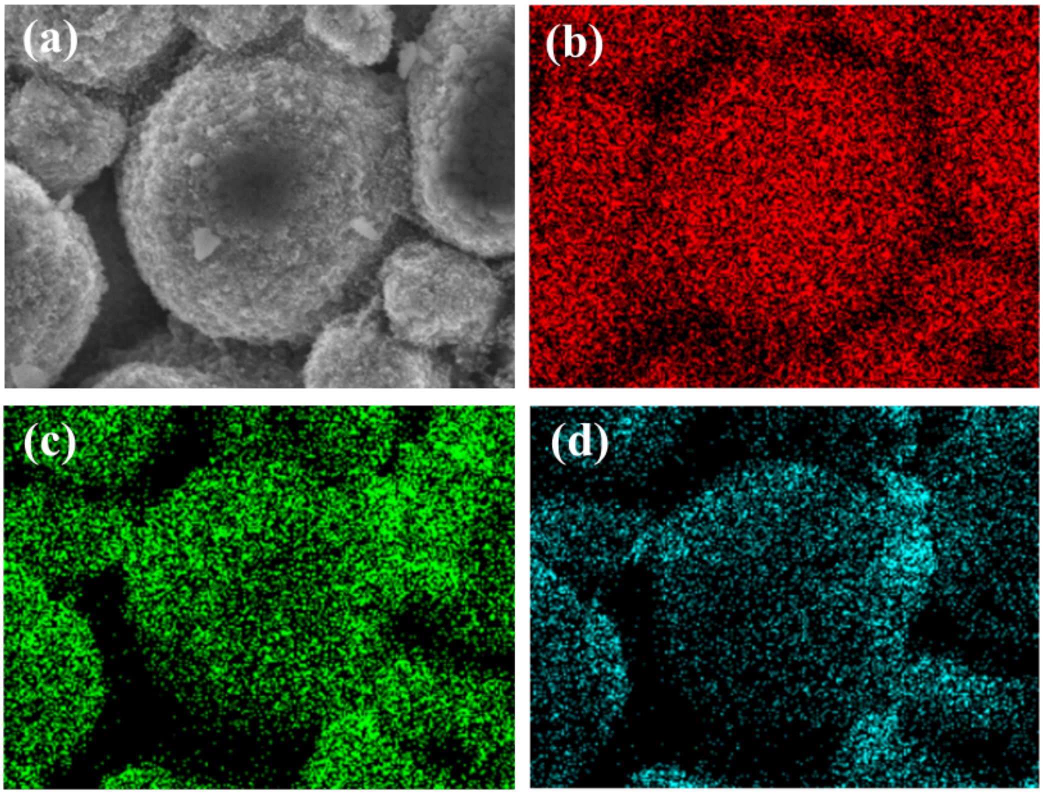

Fig. S3 SEM-EDS mapping of an electrode coated with 50 ALD cycles showing (a) SEM image, (b) Ni signal, (c) Al signal, and (d) C signal.

Table S3 Elemental composition determined by SEM-EDS according to Fig. S3.

Element	Line Type	Apparent Concentration	k Ratio	Wt%	Wt% Sigma
C	K series	0.14	0.00138	13.59	0.20
O	K series	1.35	0.00453	22.71	0.15
F	K series	0.21	0.00041	3.00	0.10
Al	K series	0.12	0.00085	3.95	0.06
Si	K series	0.00	0.00000	0.00	0.00
Ti	K series	0.02	0.00021	0.51	0.05
Mn	K series	0.25	0.00249	5.86	0.11
Co	K series	0.25	0.00250	6.59	0.15
Ni	K series	1.71	0.01715	43.79	0.25
Total:				100.00	

Table S4 Coating thickness measured from HRTEM images for NMC, NMC-10ALD, NMC-25ALD, and NMC-50ALD samples, as shown in Fig 3.

Number of ALD cycles	Thickness (nm)
0	0
10	2.42
25	3.37
50	7.40

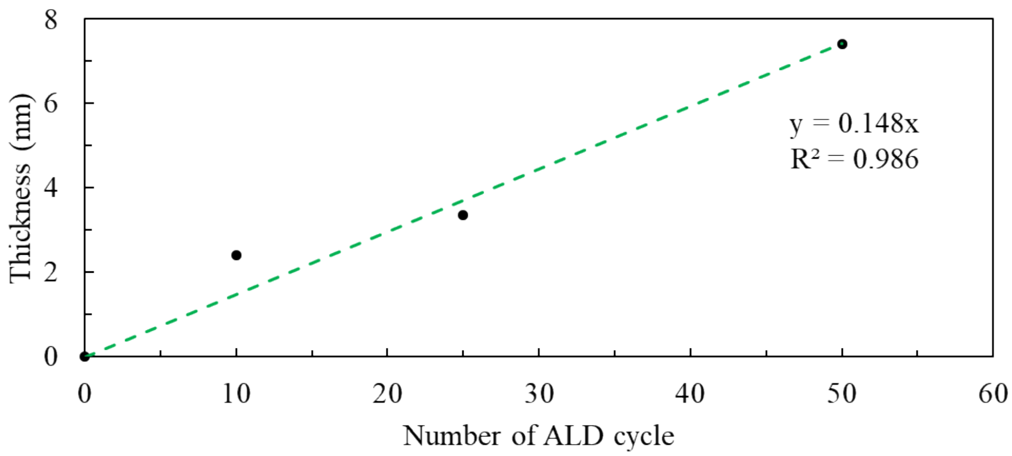

Fig. S4 Relationship between coating thickness determined from HRTEM and the number of ALD cycles, illustrating the growth rate of the alumina layer per cycle.

Table S5 Summary of growth rates of Al_2O_3 deposited by ALD on layered oxide cathodes from previous studies.

Active Material	Type of Substrate	Growth Rate ($\dot{A}$/cycle)	Temperature (°C)	Reference
LCO	Particle	2.2, 2	180	[1, 2]
	Electrode	2.2, 1	180	[1, 3]
		1.3	150	[4]
NMC111	Particle	1.3	180	[5]
		2.2	120	[6]
	Electrode	0.99	85	[7]
NMC442	Electrode	1.1-1.5	120	[8]
NMC532	Particle	1.2	200	[9]
		1	100	[10]
	Electrode	1.1	180	[11]
		1.0-3.0	120	[12]
NMC622	Particle	1.3	110	[13]
		1.1-1.2	100	[14]
	Electrode	1	120	[15]
NMC70	Electrode	1	120	[15]
NMC811	Electrode	1	120	[15]

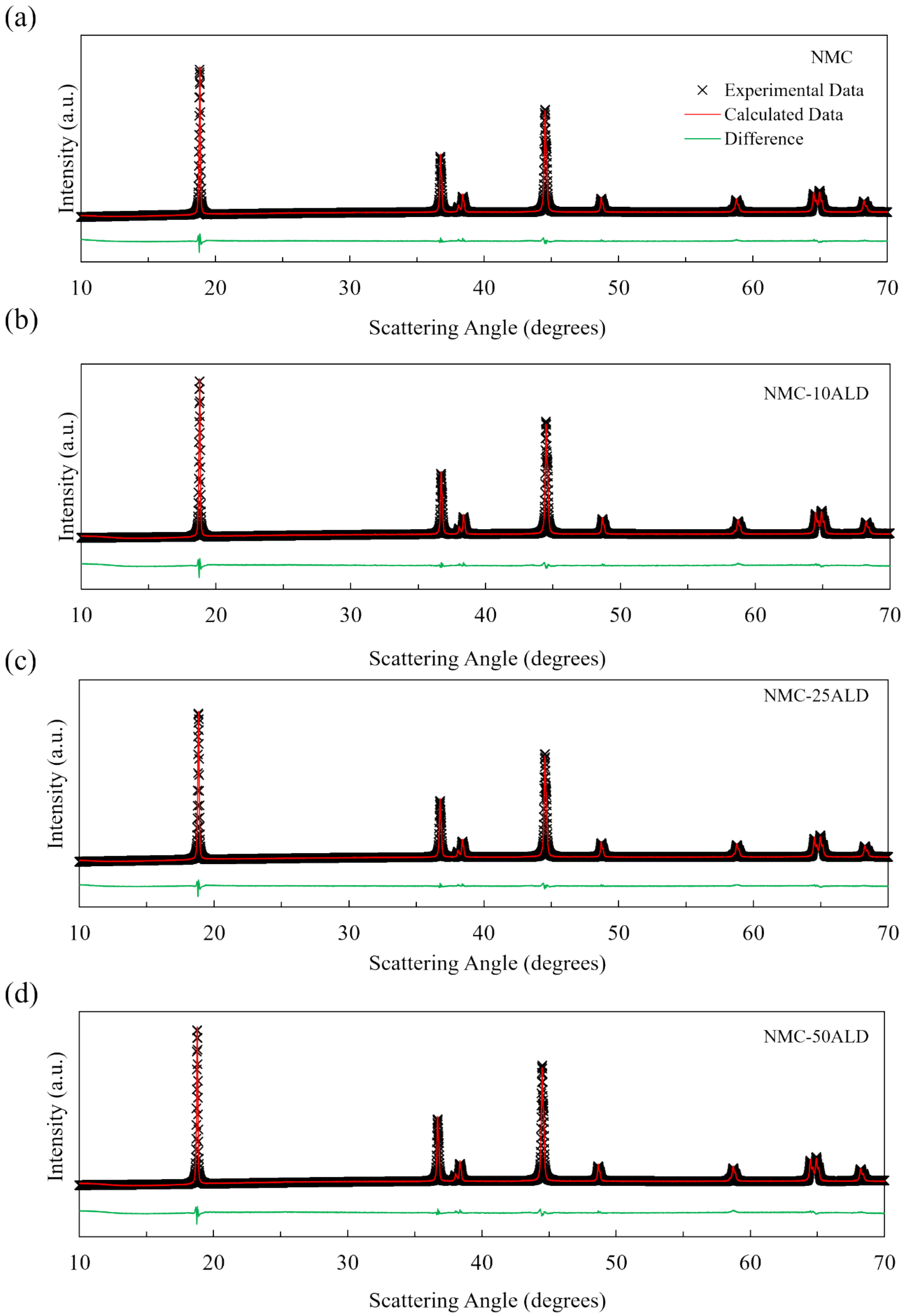

Fig. S5 XRD diffraction patterns of (a) NMC811, (b) NMC-10ALD, (c) NMC-25ALD, and (d) NMC-50ALD, along with the corresponding Rietveld refinement results.

Table S6. Lattice parameters obtained from Rietveld refinement for NMC, NMC-10ALD, NMC-25ALD, and NMC-50ALD, corresponding to the XRD patterns shown in Fig. S5.

	Lattice parameters			
	a ($\dot{A}$)	c ($\dot{A}$)	%Ni in Li layer	R_{bragg}
NMC	2.8726	14.2008	2.656	1.11
NMC-10ALD	2.8721	14.1992	2.926	1.21
NMC-25ALD	2.8721	14.2000	2.576	0.97
NMC-50ALD	2.8721	14.1997	3.090	1.37

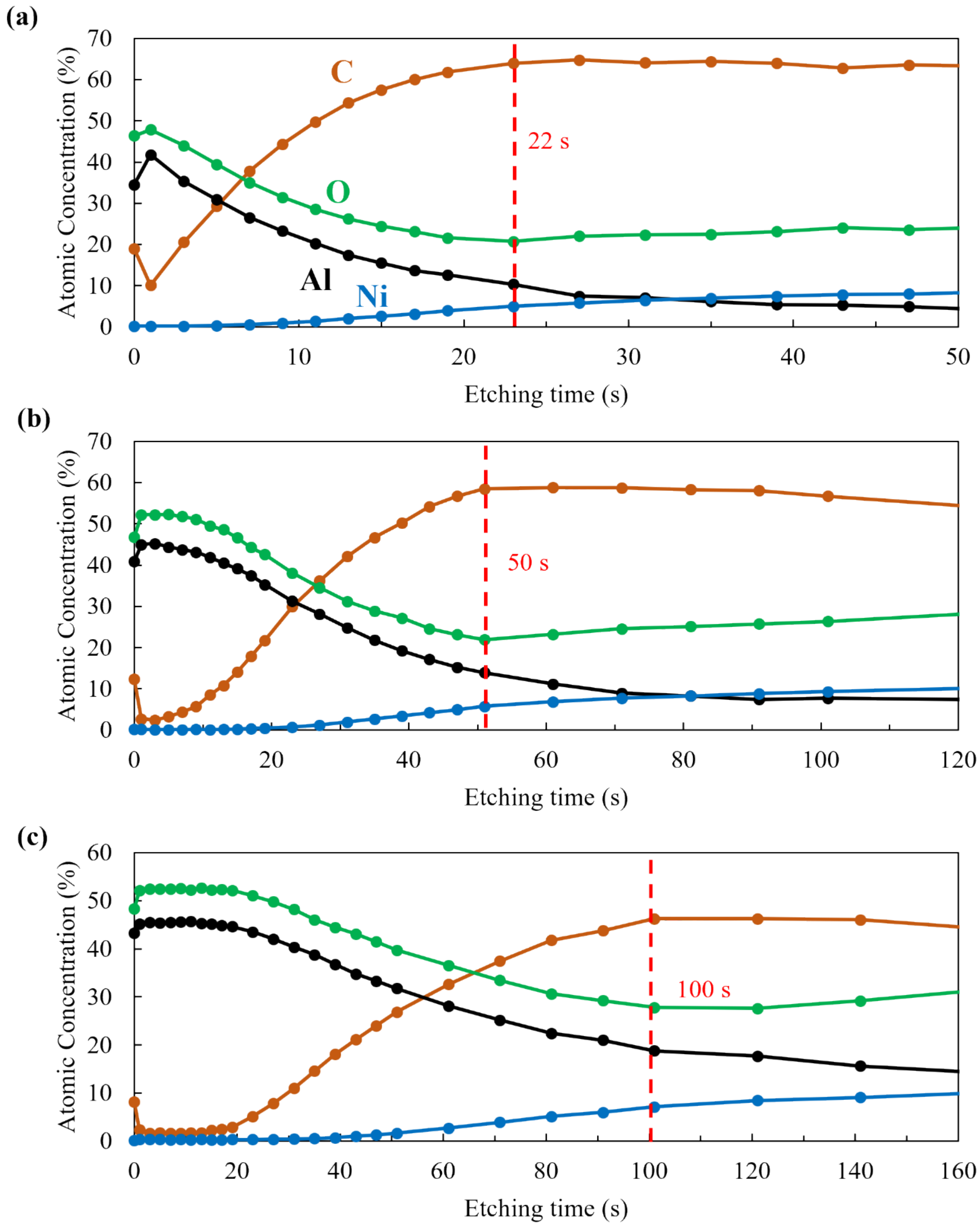

Fig. S6 XPS depth profiles of (a) NMC-10ALD, (b) NMC-25ALD, and (c) NMC-50ALD, displaying the atomic concentrations calculated from C 1s, O 1s, Al 2p, and Ni 2p3/2 signals. The dashed lines represent the thickness of the primary Al_2O_3 layer.

Table S7. Coating thickness (etching time) determined from XPS analysis, as illustrated in Fig. S6.

Number of ALD cycle	Ar Bombard (s)
0	0
10	22
25	50
50	100

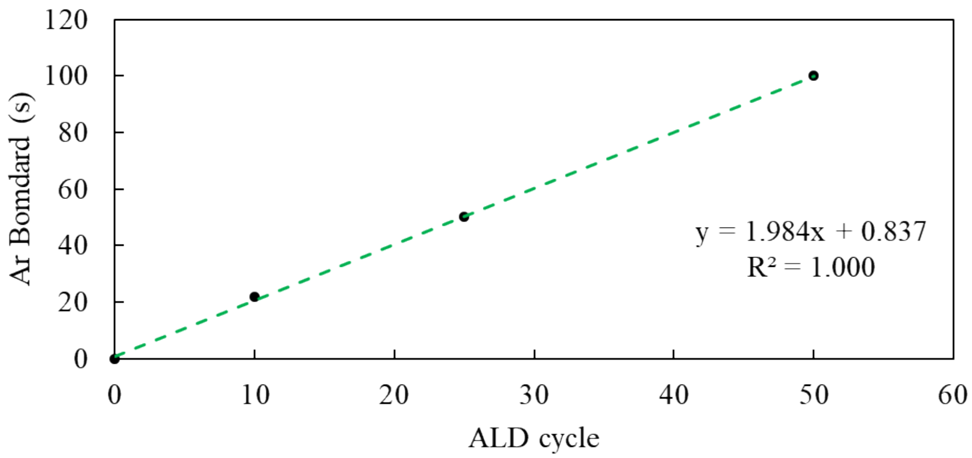

Fig. S7 Relationship between etching time, representing coating thickness as determined from XPS, and the number of ALD cycles, illustrating the growth rate of the alumina layer.

Table S8. Properties of NMC811 and graphite electrodes for 18650 cylindrical cells.

Electrode properties	Anode: Graphite	Coating thickness = 230 µm
		Electrode thickness = 130 µm (Pressing 6.5 tons)
		Active mass = 9.92 g
	Cathode: NMC811	Coating thickness = 215 µm
		Electrode thickness = 145 µm (Pressing 9 tons)
		Active mass = 14.63 g
N-to-p ratio	1.20 (NMC811 = 180 mAh/g, Graphite = 320 mAh/g)	
Cell weight	41.60 g	
Electrolyte	1.2 M $LiPF_6$ in FEC: DMC (1: 4, v/v) 4.63 g	
Cell Capacity	2,373 mAh (0.1C) 2,319 mAh (0.2C)	
Nominal voltage	3.67 V	
Energy density	Volumetric 544 Wh/L_{cell} (16 ml) Gravimetric 209 Wh/kg_{cell} 595 Wh/kg_{NMC}	
Internal resistance	18.2 mΩ	

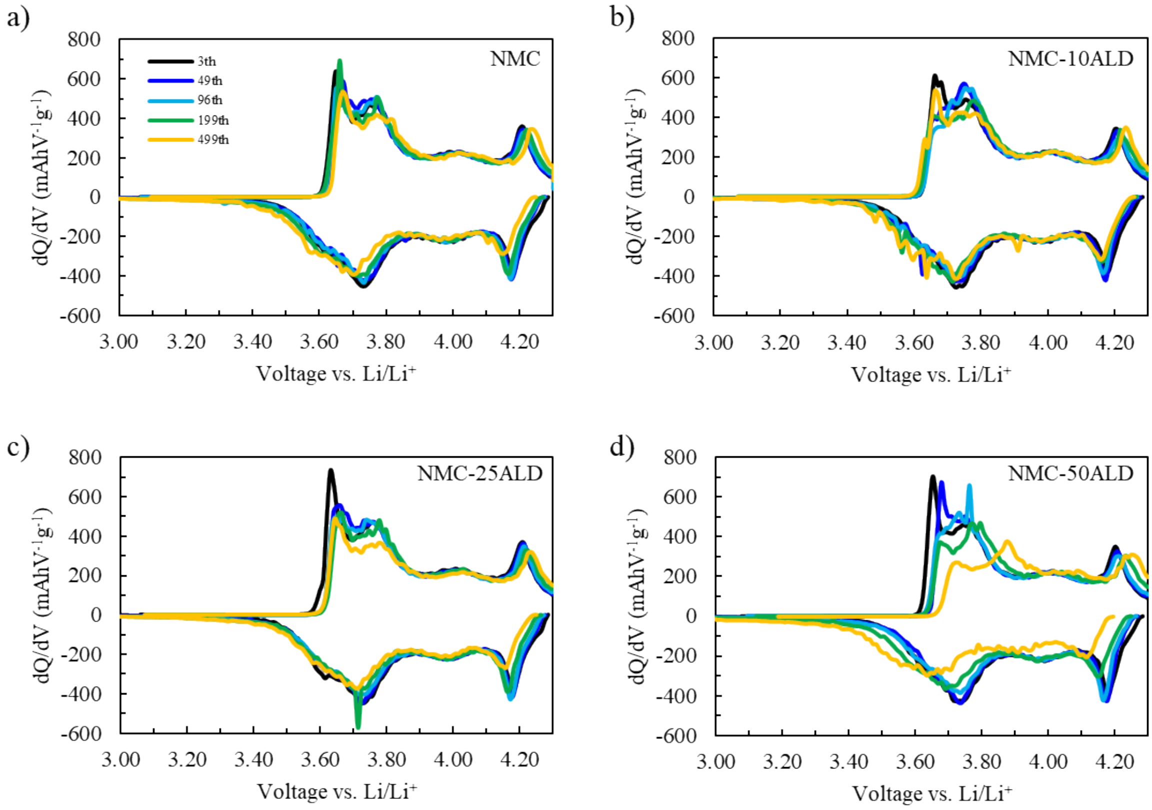

Fig. S8 dQ/dV peak of (a) NMC, (b) NMC-10ALD, (c) NMC-25ALD, and (d) NMC-50ALD at checkup cycle at C/20 in the voltage range of 3.0-4.3V.

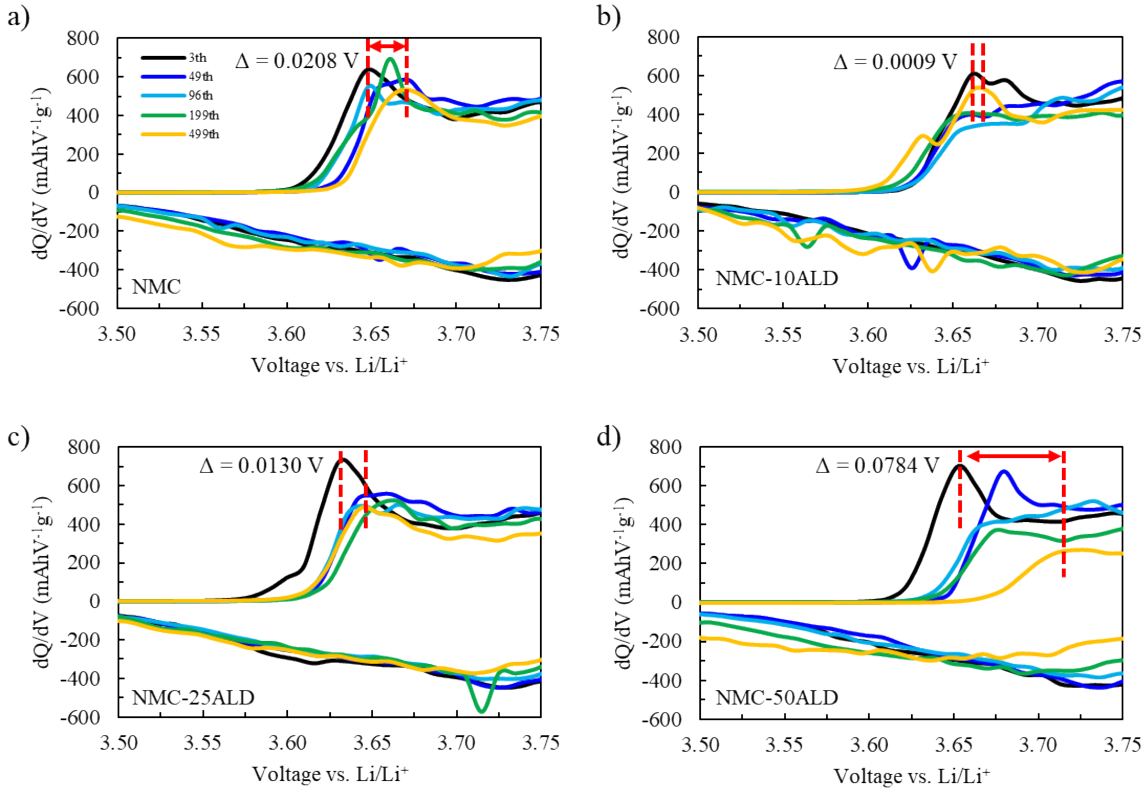

Fig. S9 dQ/dV peak enlarged at H1-M peak position of (a) NMC, (b) NMC-10ALD, (c) NMC-25ALD, and (d) NMC-50ALD at checkup cycle at C/20 in voltage range of 3.0-4.3V.

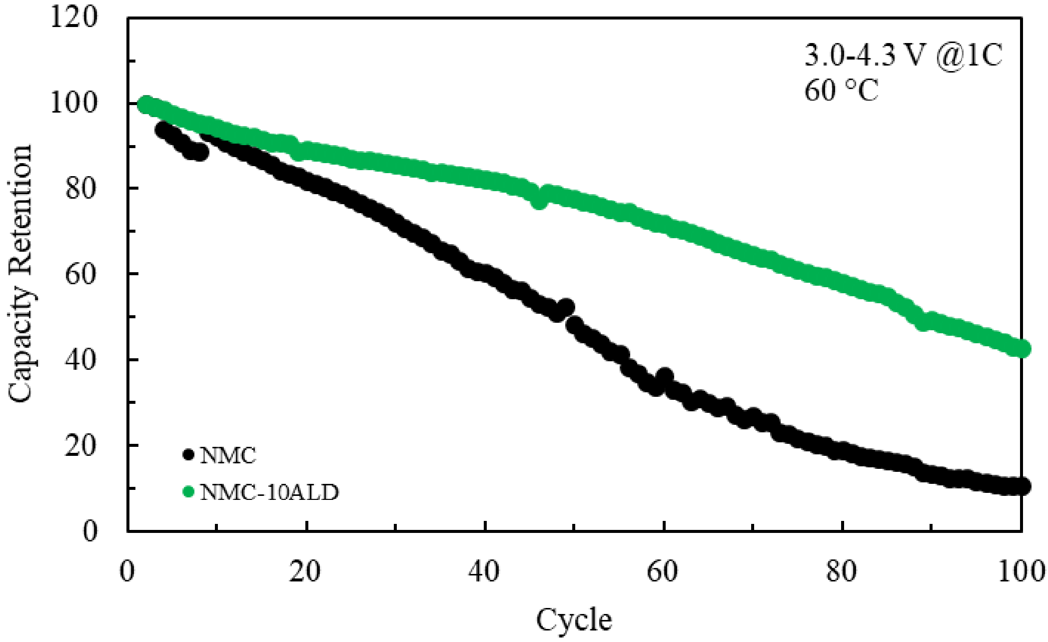

Fig. S10 Capacity retention of NMC and NMC-10ALD testing at 60°C in voltage range of 3.0-4.3V at 1C.

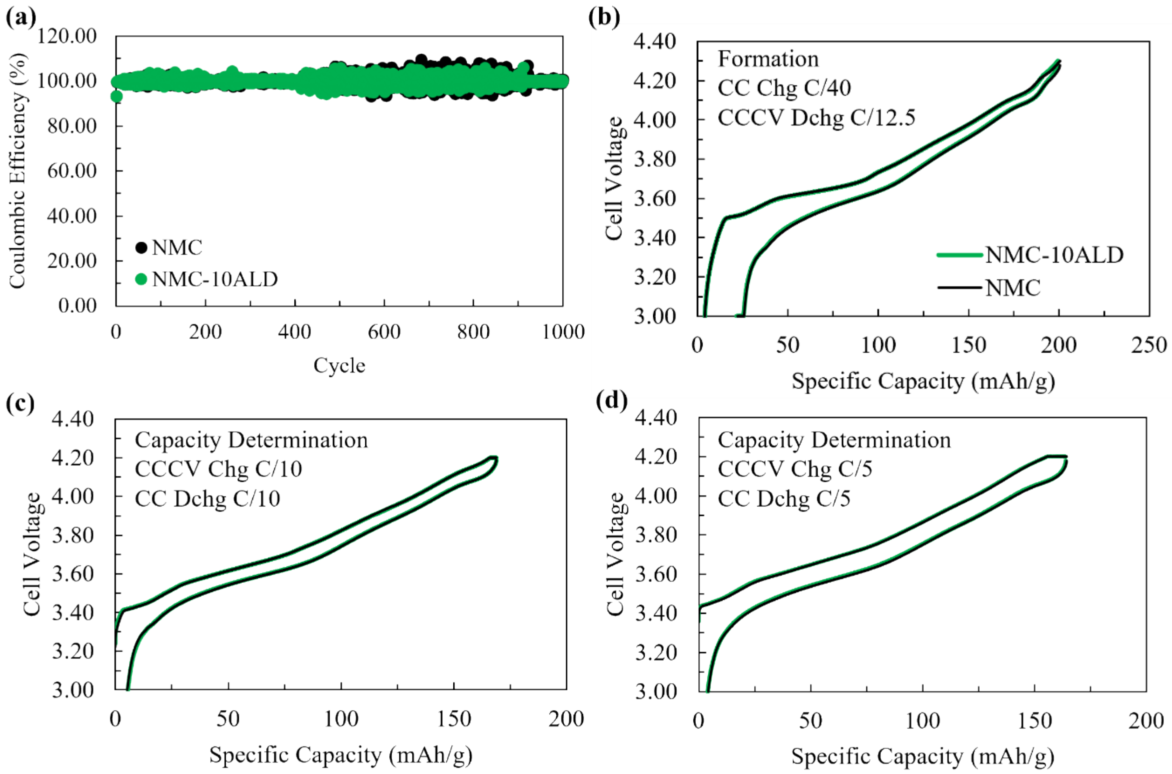

Fig. S11 Electrochemical performance of 18650 cylindrical cells of NMC and NMC-10ALD as cathode couple with graphite anode: (a) coulombic efficiency, (b) charge-discharge profile of formation cycle, (c) charge-discharge profile of capacity determination at C/10, and (d) charge-discharge profile of capacity determination at C/5.

Table S9. Summarized electrochemical performance of various coating strategies applied on NMC series cathode.

Coating Technique	Coating Material	Active Material	Testing Condition	Capacity Retention	Configuration	Reference
This work ALD	Al_2O_3	NMC811	3.0-4.3 0.5C	52.88% @499cycle	Half cell Coin cell	-
			3.0-4.2 Chg 0.5C Dchg 1C	71.20% @1,000cycle	Full cell 18650	
ALD	Al_2O_3	NMC532	3.0-4.6 V 1C	75.5% @ 100cycle	Half cell Coin cell	[11]
ALD	Al_2O_3	NMC811	-	76.3% @600cycle	Full cell Coin cell	[16]
			2.7-4.3 1C	88.0%@300	Half cell Coin cell	
ALD	Al_2O_3	NMC622	2.8-4.2 V CCCV 1C	85.3% @1,400	Full cell Coin cell	[13]
ALD	Al_2O_3	NMC532	3.0-4.3V Chg C/3 Dchg 1C	~90% @180cycle	Half cell Coin cell	[9]
ALD	Al_2O_3	LCO	3.3-4.5V 1C	89% @120cycle	Half cell Coin cell	[1]
ALD	Al_2O_3	NMC111	3.0-4.5V 1C	96% @100cycle	Half cell Coin cell	[5]
ALD	Al_2O_3	NMC532	3.0-4.3V C/5	92.1% @100cycle	Half cell Coin cell	[10]
ALD	Al_2O_3	NMC532	3.0-4.5V 0.5C	85% @100cycle	Half cell Coin cell	[12]
ALD	Al_2O_3	NMC622	3.0-4.3V 0.5C	94.5% @45cycle	Half cell Coin cell	[14]
Dry coating	Al_2O_3	NMC811	3.0-4.2V 0.5C	77.4% @300cycle	Full cell 18650	[17]
			2.7-4.3 V 1C	86.5% @100cycle	Half cell Coin cell	
Dry coating	Al_2O_3	NMC70 1515	3.0-4.3V 0.5C	92% @100cycle	Half cell Coin cell	[18]
Wet coating	Al_2O_3	LNO	3.0-4.3V C/3	96% @200cycle	Half cell Coin cell	[19]
Wet coating	Al_2O_3	NMC811	2.8-4.3V 1C	98.31% @200cycle	Half cell Coin cell	[20]
Dry coating	$Al(OH)_3$	NMC811	2.75-4.3V 1C	87.6% @200cycle	Half cell Coin cell	[21]
ball milling mixing and solid-phase synthesis	$LiAlO_2/Al(OH)_3$	NMC811	2.5-4.3V 1C	93.90% @200cycle	Half cell Coin cell	[22]

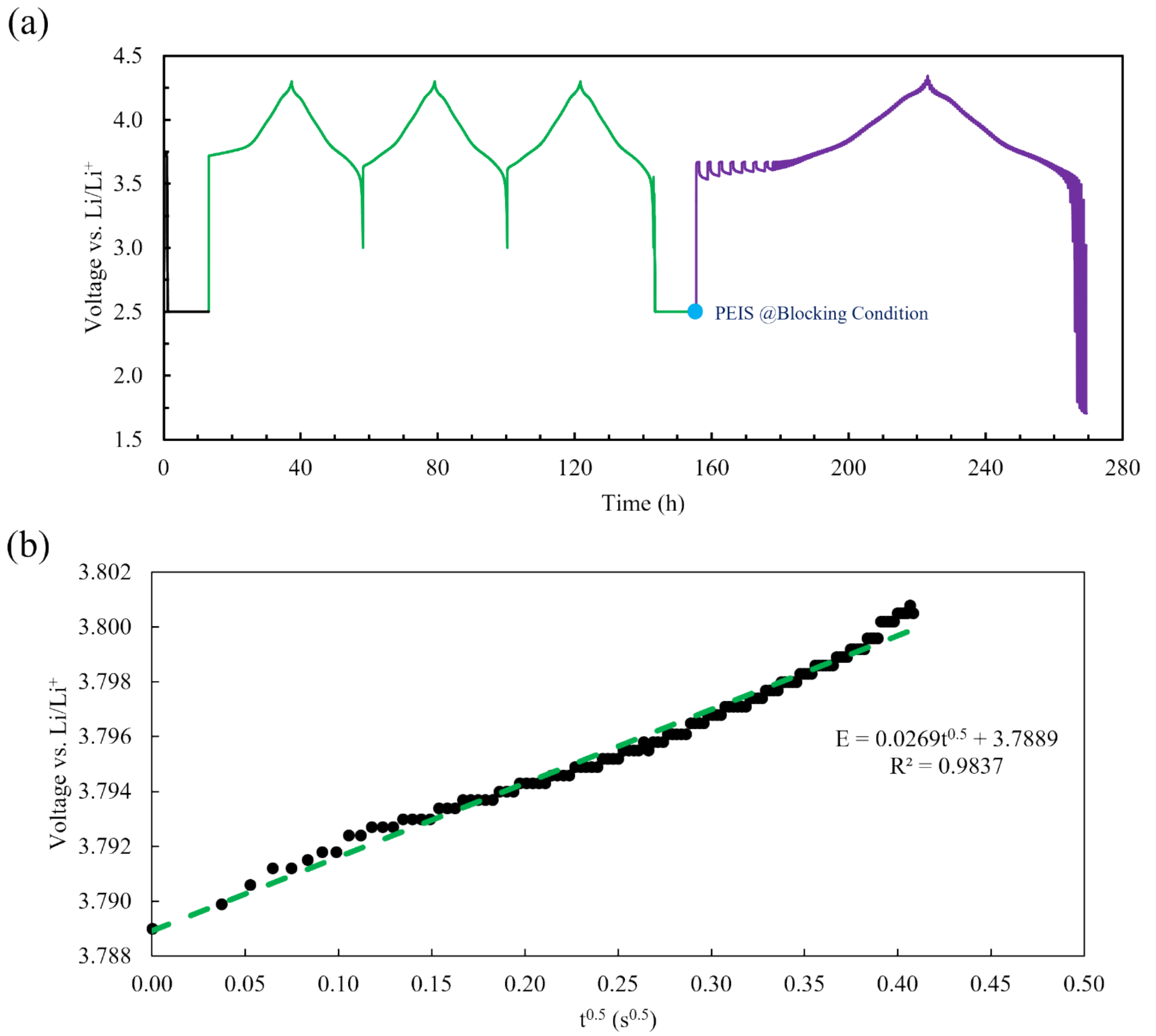

Fig. S12 The galvanostatic intermittent titration technique (GITT) step: (a) The procedure of GITT measurement coupled with capacitance measurement, including the conditioning step (black), formation steps (green), and GITT step (purple). (b) The relationship between cell voltage and $\tau^{1/2}$.

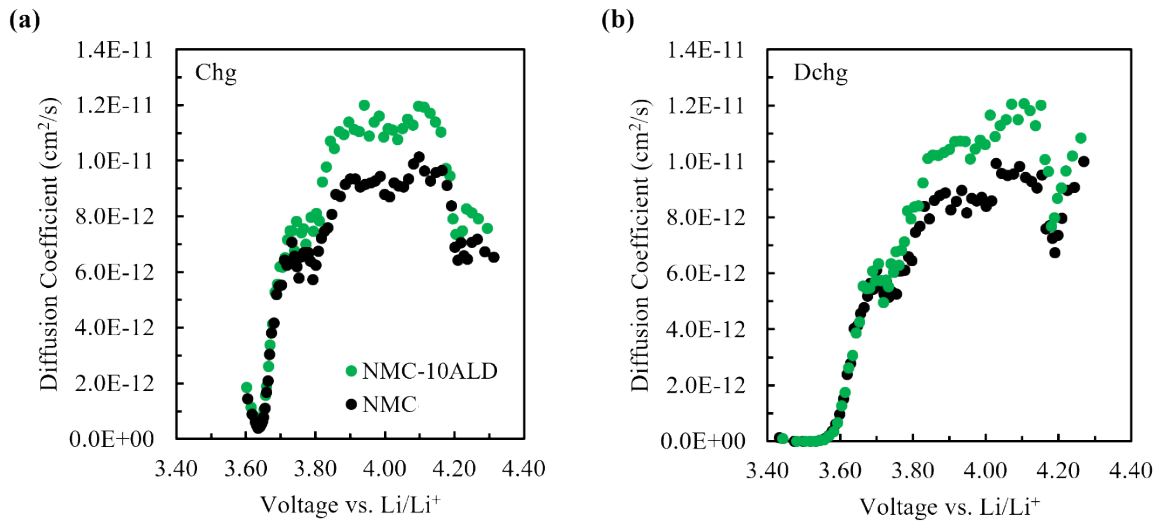

Fig. S13 Lithium-ion diffusion coefficient calculated from GITT as a function of voltage during (a) charge and (b) discharge.

Link to Video S1. Jelly roll 18650 cylindrical cells during formation cycle followed by electrochemical abuse at 4.3, 4.6, and 4.9 V of NMC and NMC-10ALD.

https://www.dropbox.com/scl/fi/cgo2u9adtdn816op79b4i/VDO_S1.mp4?rlkey=sxuqcbxv73vfyqf75m9iihkyq&st=otg3f00b&dl=0

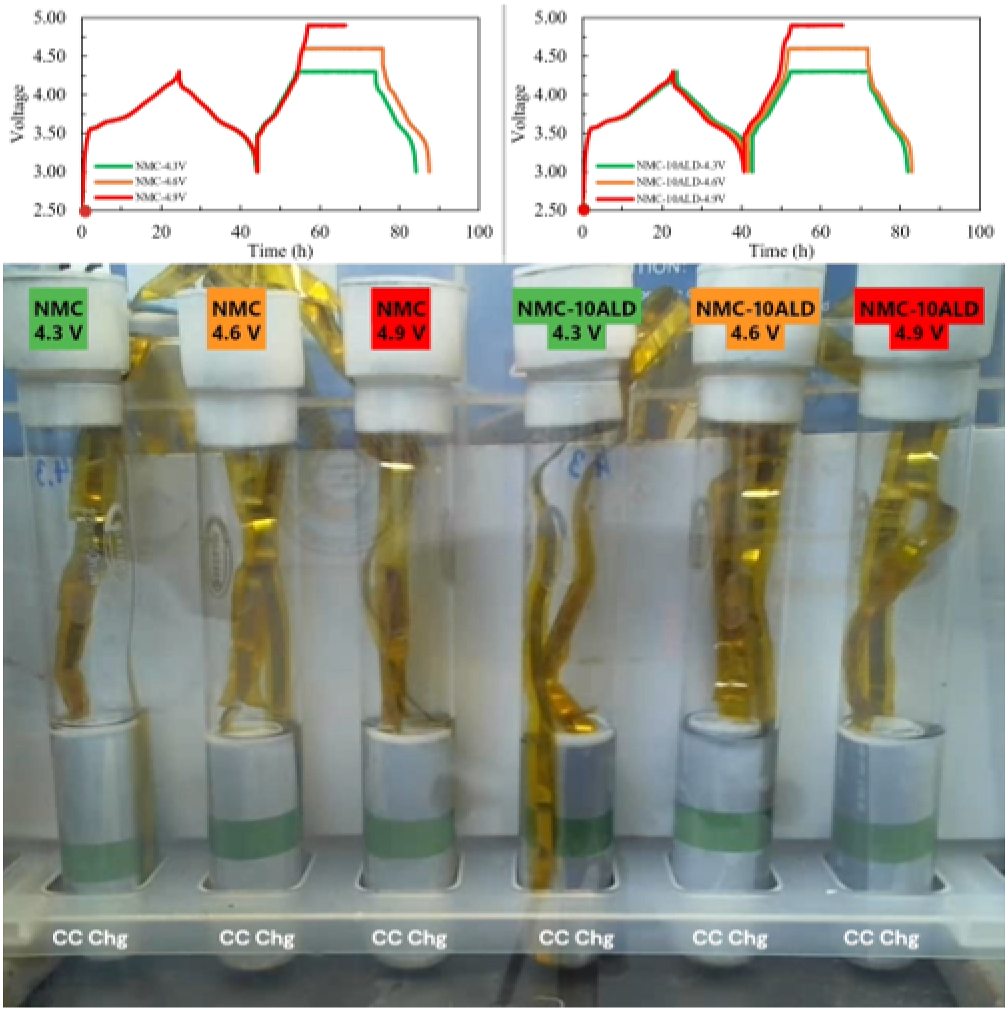

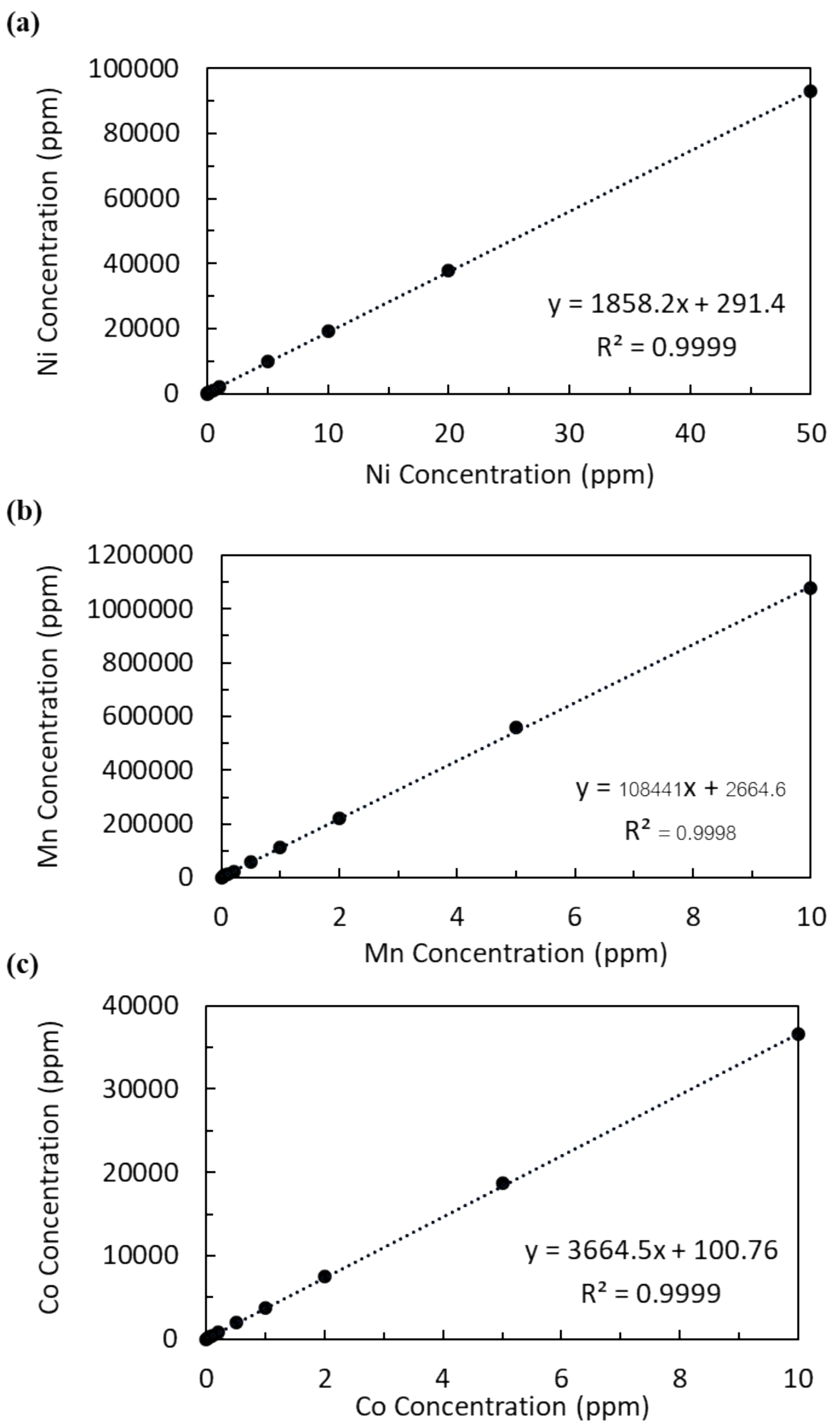

Fig. S14 Calibration curve of transition metal dissolution used to determine the elemental concentration in ICP-OES for (a) Ni, (b) Mn, and (c) Co.

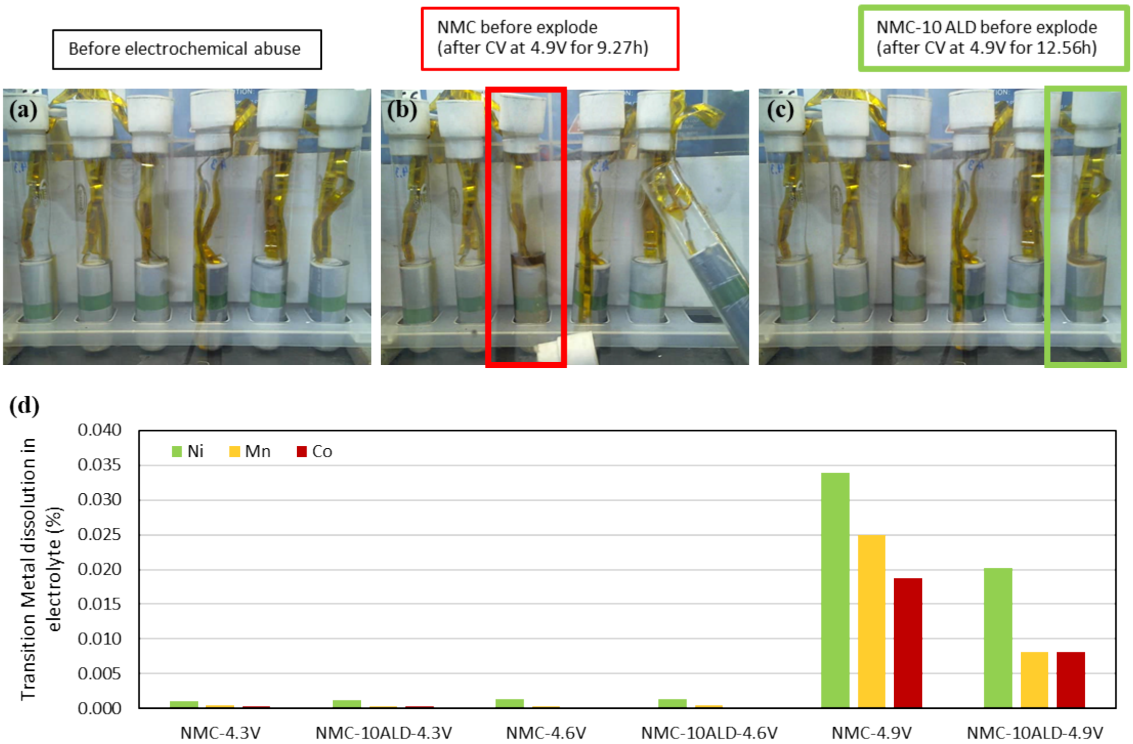

Fig. S15 The jelly roll showing color of electrolyte at (a) before abuse, (b) before explosion of NMC after abused at 4.9V, and (c) before explosion of NMC-10ALD after abused at 4.9V. (d) Transition metal dissolution in electrolyte

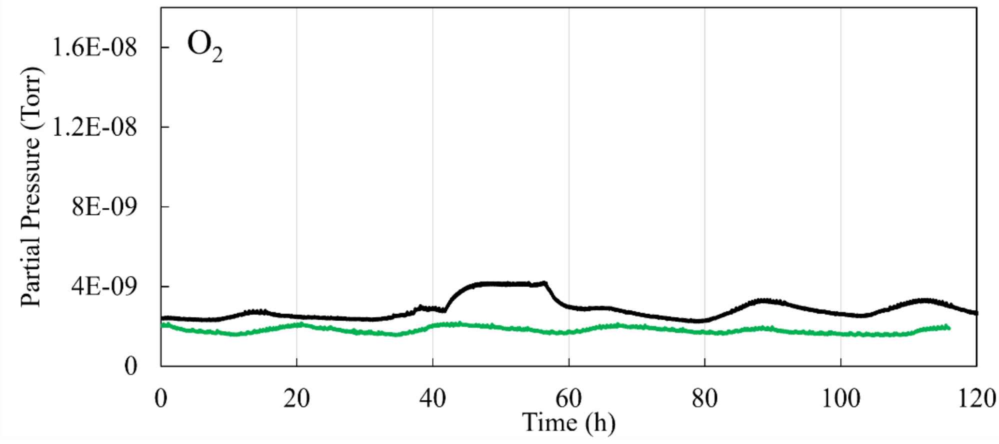

Fig. S16 Oxygen signal detected from DEMS measurement

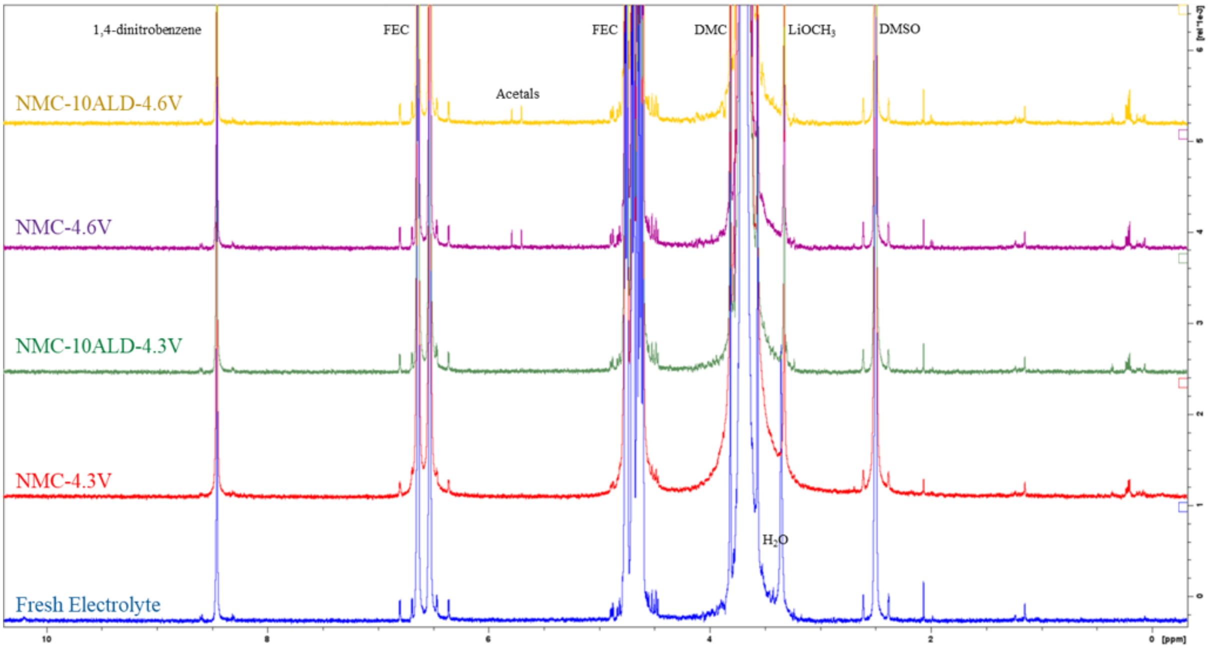

Fig. S17 1H NMR spectra of fresh electrolyte (blue) and electrolyte collecting from the jelly roll according to experimental shown in Fig. 5 including NMC and NMC-10ALD after abused at 4.3V (red and green), and 4.6V (purple and yellow), respectively.

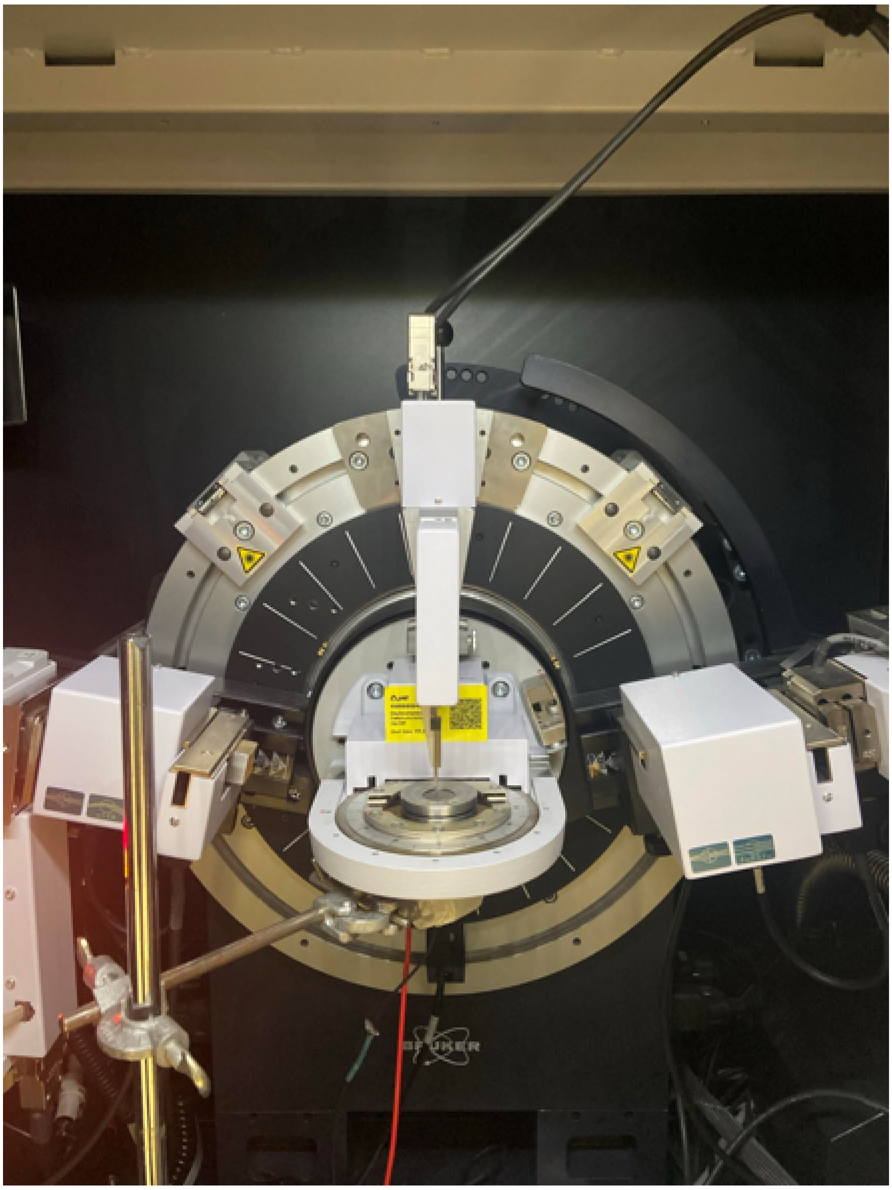

Fig. S18 Experimental set-up of *in situ* XRD.

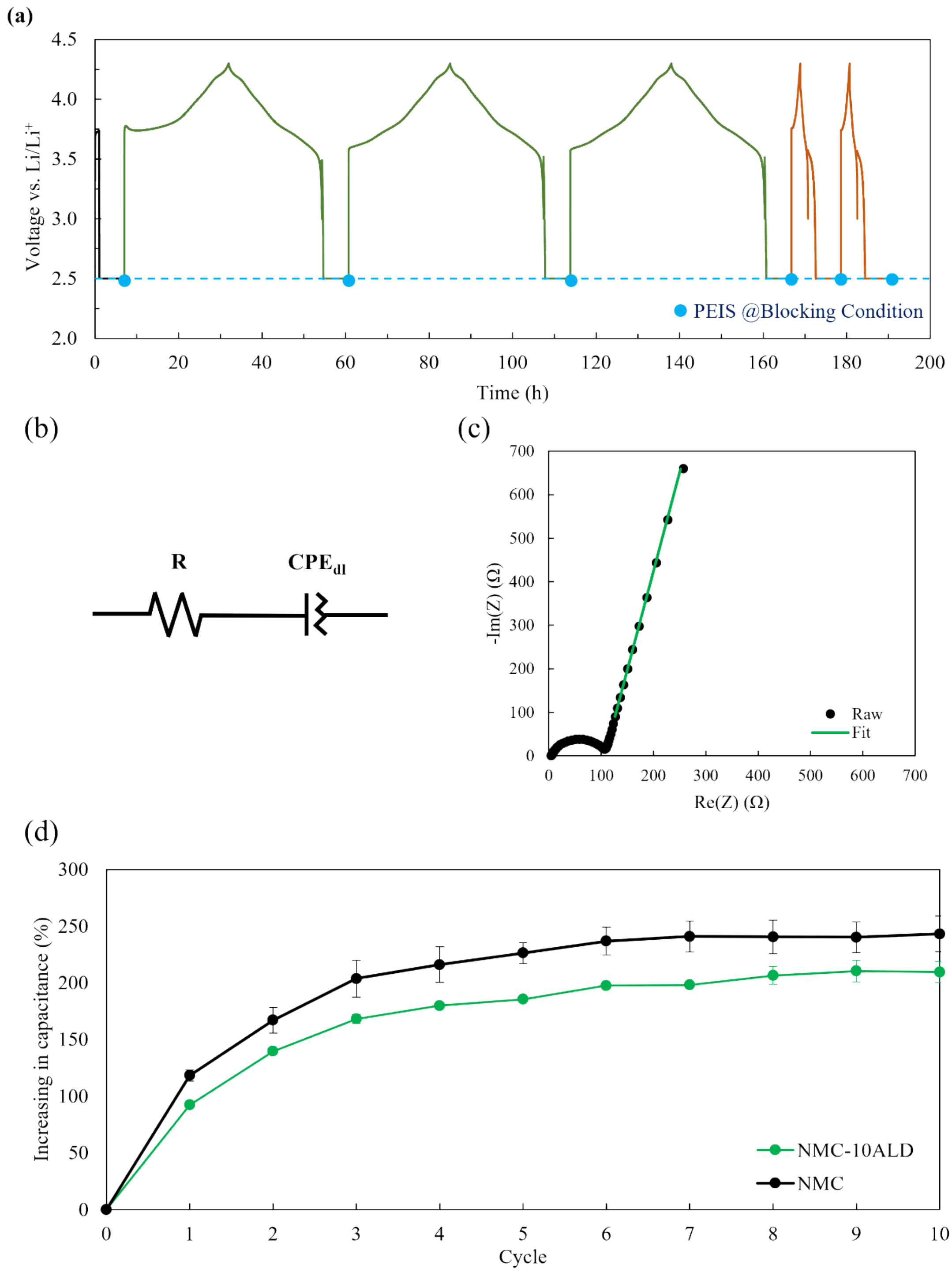

Fig. S19 The capacitance measurement for surface area change investigation. (a) The procedure of capacitance measurement includes the conditioning step (black), formation (green), and cycling (orange) before holding CV at 2.5 V, followed by PEIS, illustrated as blue dots. (b) Equivalent circuit used to fit the EIS spectra in the frequency range of 1 Hz – 100 mHz. (c) example of Nyquist plot shows the experimental data (black dot) and the fitting result (green line). (d) The percentage of increase in capacitance with respect to their capacitance before testing (after conditioning) of NMC and NMC-10ALD.

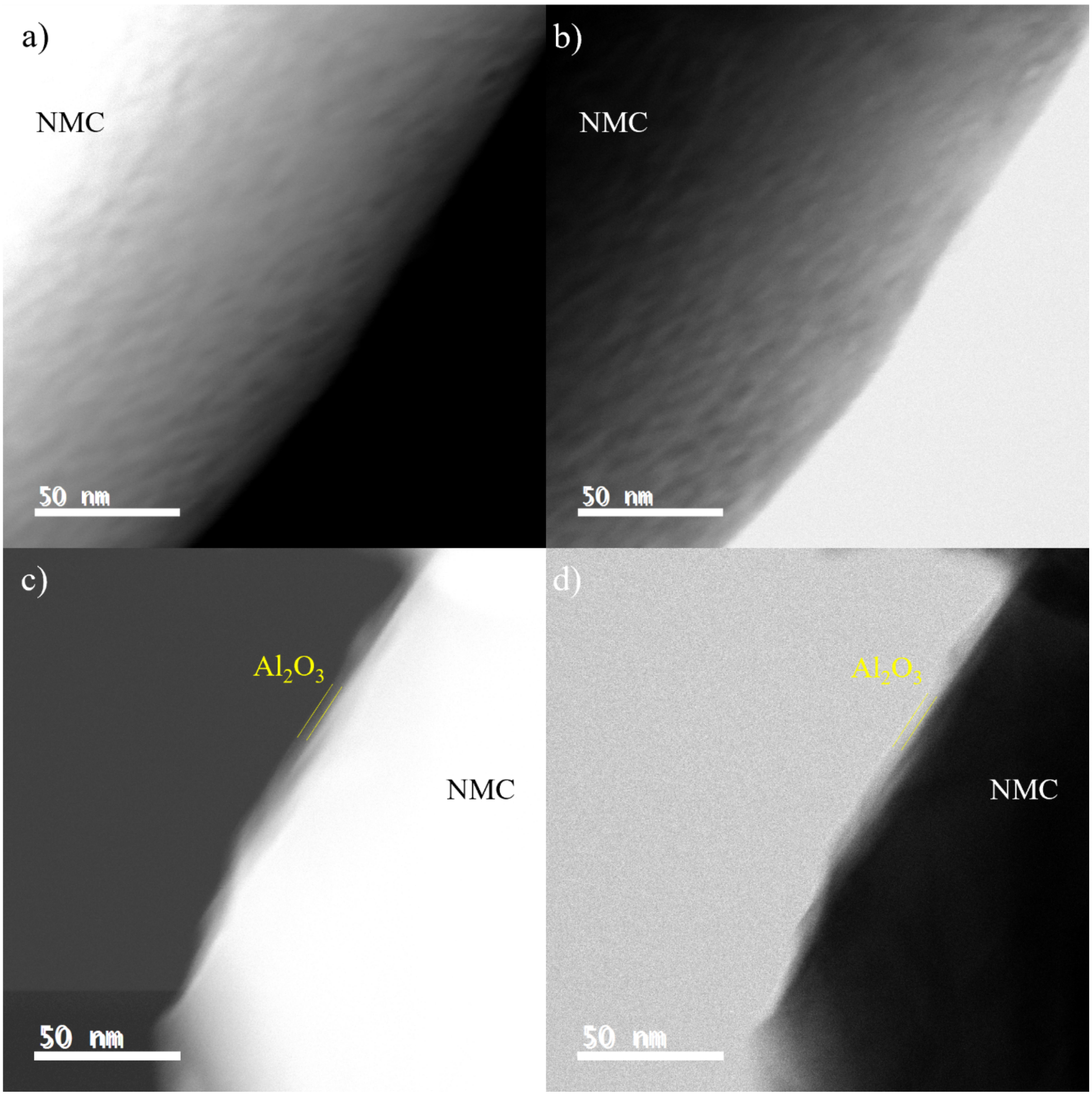

Fig. S20 STEM images show (a)HAADF-STEM and (b)BF-STEM image of NMC and(c)HAADF-STEM and (d)BF-STEM image of NMC-10ALD after electrochemical stability test for 1,000 cycles.

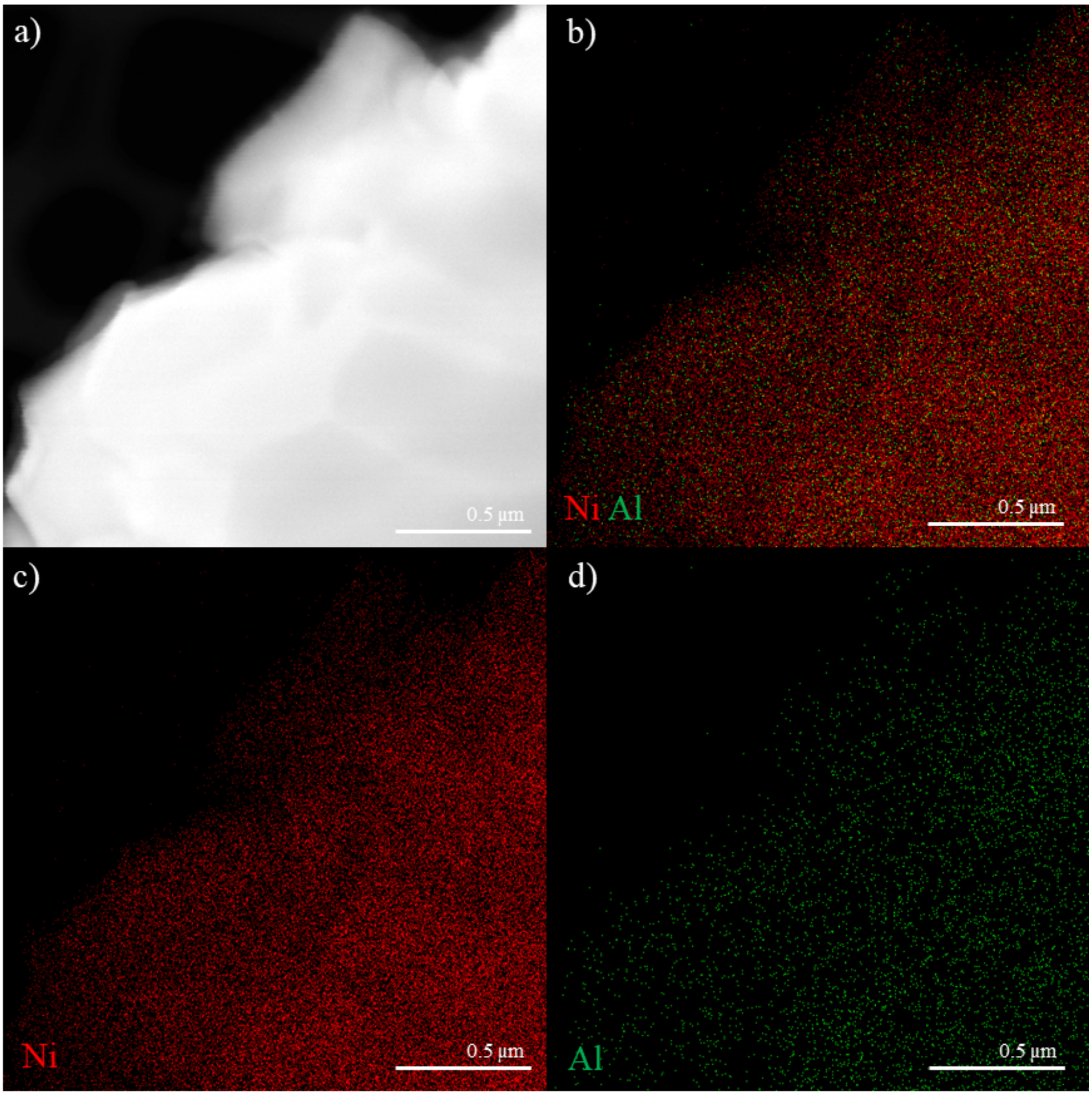

Fig. S21 STEM-EDS mapping of NMC-10ALD after electrochemical stability test for 1,000 cycle showing (a) STEM image of mapped area, (b) overlapping of Al and Ni signal with individual mapping of (c) Ni and (d)Al.

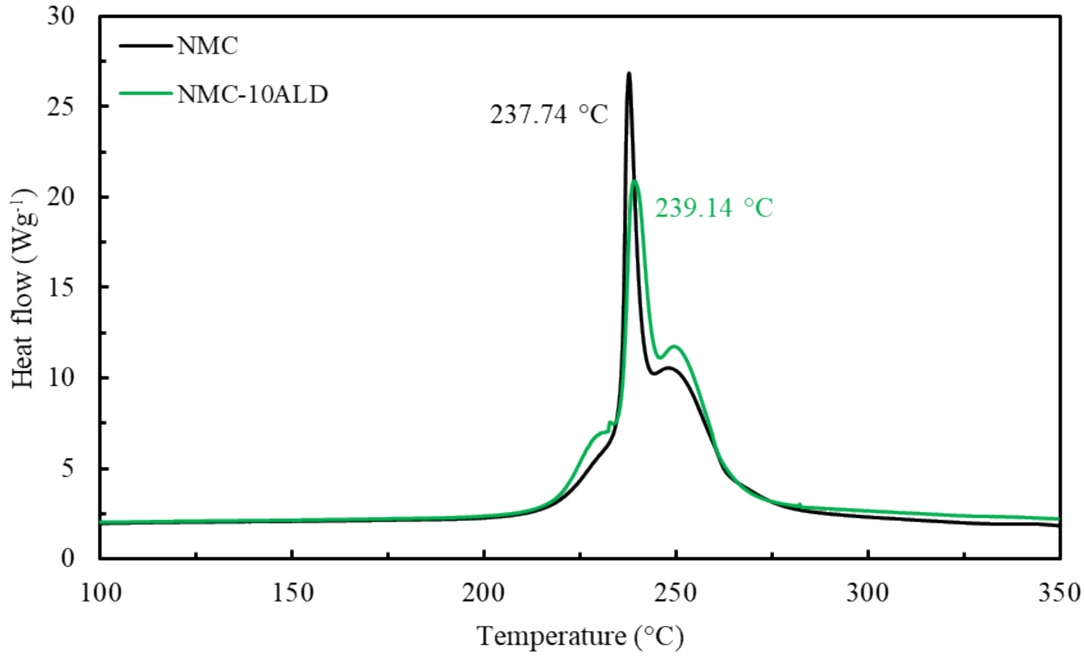

Fig. S22 DSC curves of NMC and NMC-10ALD collected after 1,000 cycles at charged state.

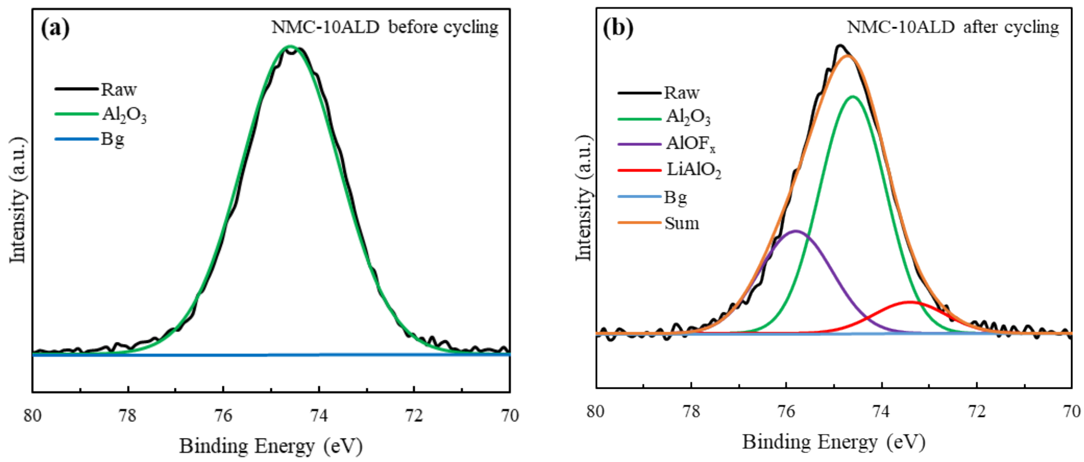

Fig. S23 XPS spectrum of Al 2p for (a)fresh NMC-10ALD and (b)cycled NMC-10ALD

References

1. Y. S. Jung, A. S. Cavanagh, A. C. Dillon, M. D. Groner, S. M. George and S.-H. Lee, *Journal of The Electrochemical Society*, 2010, 157, A75.
2. M. Xie, T. Hu, L. Yang and Y. Zhou, *RSC Advances*, 2016, 6, 63250-63255.
3. Q. Cheng, T. Yang, Y. Li, M. Li and C. K. Chan, *Journal of Materials Chemistry A*, 2016, 4, 6902-6910.
4. X. Li, J. Liu, X. Meng, Y. Tang, M. N. Banis, J. Yang, Y. Hu, R. Li, M. Cai and X. Sun, *Journal of Power Sources*, 2014, 247, 57-69.
5. J. W. Kim, J. J. Travis, E. Hu, K.-W. Nam, S. C. Kim, C. S. Kang, J.-H. Woo, X.-Q. Yang, S. M. George, K. H. Oh, S.-J. Cho and S.-H. Lee, *Journal of Power Sources*, 2014, 254, 190-197.
6. A. L. Hoskins, W. W. McNeary, S. L. Millican, T. A. Gossett, A. Lai, Y. Gao, X. Liang, C. B. Musgrave and A. W. Weimer, *ACS Applied Nano Materials*, 2019, 2, 6989-6997.
7. A. K. Haridas, Q. A. Nguyen, B. F. Song, R. Blaser and S. L. Biswal, *ACS Applied Energy Materials*, 2020, 3, 456-468.
8. A. M. Wise, C. Ban, J. N. Weker, S. Misra, A. S. Cavanagh, Z. Wu, Z. Li, M. S. Whittingham, K. Xu, S. M. George and M. F. Toney, *Chemistry of Materials*, 2015, 27, 6146-6154.
9. M. R. Laskar, D. H. K. Jackson, S. Xu, R. J. Hamers, D. Morgan and T. F. Kuech, *ACS Applied Materials & Interfaces*, 2017, 9, 11231-11239.
10. D. H. K. Jackson and T. F. Kuech, *Journal of Power Sources*, 2017, 365, 61-67.
11. Y. Shi, M. Zhang, D. Qian and Y. S. Meng, *Electrochimica Acta*, 2016, 203, 154-161.
12. Y. Su, S. Cui, Z. Zhuo, W. Yang, X. Wang and F. Pan, *ACS Applied Materials & Interfaces*, 2015, 7, 25105-25112.
13. S. Neudeck, A. Mazilkin, C. Reitz, P. Hartmann, J. Janek and T. Brezesinski, *Scientific Reports*, 2019, 9, 5328.
14. X. Wang, J. Cai, Y. Liu, X. Han, Y. Ren, J. Li, Y. Liu and X. Meng, *Nanotechnology*, 2021, 32, 115401.
15. R. S. Negi, S. P. Culver, M. Wiche, S. Ahmed, K. Volz and M. T. Elm, *Physical Chemistry Chemical Physics*, 2021, 23, 6725-6737.
16. L. Wang, Q. Su, W. Shi, C. Wang, H. Li, Y. Wang, G. Du, M. Zhang, W. Zhao, S. Ding and B. Xu, *Electrochimica Acta*, 2022, 435, 141411.

17. K. Srimanon, S. Vadivel and M. Sawangphruk, *Journal of Power Sources*, 2022, 550, 232150.
18. M. J. Herzog, N. Gauquelin, D. Esken, J. Verbeeck and J. Janek, *Energy Technology*, 2021, 9, 2100028.
19. A. R. Haworth, B. I. J. Johnston, L. Wheatcroft, S. L. McKinney, N. Tapia-Ruiz, S. G. Booth, A. J. Nedoma, S. A. Cussen and J. M. Griffin, *ACS Applied Materials & Interfaces*, 2024, 16, 7171-7181.
20. D. Hu, F. Du, H. Cao, Q. Zhou, P. Sun, T. Xu, C. Mei, Q. Hao, Z. Fan and J. Zheng, *Journal of Electroanalytical Chemistry*, 2021, 880, 114910.
21. F. Wu, Q. Shi, L. Chen, J. Dong, J. Zhao, H. Wang, F. Gao, J. Liu, H. Zhang, N. Li, Y. Lu and Y. Su, *Chemical Engineering Journal*, 2023, 470, 144045.
22. J. Wang, D. Zhao, G. Zhou, S. Wei, S. Hou, Y. Li, H. Ma, Y. Yuan, X. Yan and X. Hou, *Ceramics International*, 2023, 49, 15842-15850.